# Structural analysis of lipocalin-type prostaglandin D synthase complexed with biliverdin by small-angle X-ray scattering and multi-dimensional NMR

**ARTICLE** *in* JOURNAL OF STRUCTURAL BIOLOGY · OCTOBER 2009

Impact Factor: 3.23 · DOI: 10.1016/j.jsb.2009.10.005 · Source: PubMed

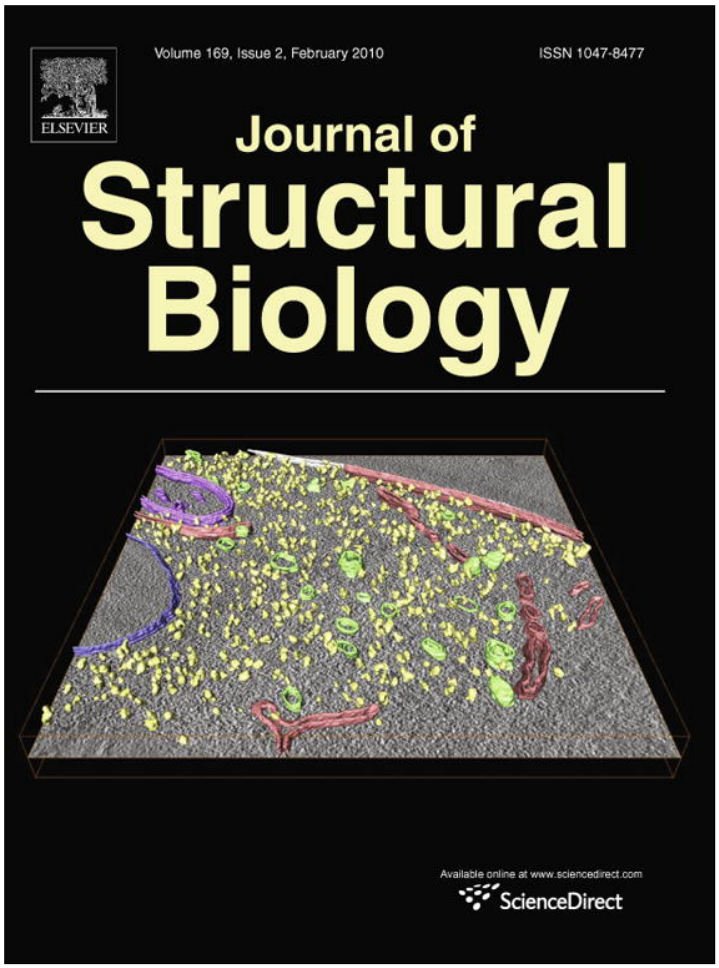

Journal of Structural Biology 169 (2010) 209–218

Contents lists available at ScienceDirect

Journal of Structural Biology

journal homepage: www.elsevier.com/locate/yjsbi

# Structural analysis of lipocalin-type prostaglandin D synthase complexed with biliverdin by small-angle X-ray scattering and multi-dimensional NMR

Yuya Miyamoto [a], Shigenori Nishimura [a], Katsuaki Inoue [b], Shigeru Shimamoto [c], Takuya Yoshida [c], Ayano Fukuhara [a], Mao Yamada [a], Yoshihiro Urade [d], Naoto Yagi [b], Tadayasu Ohkubo [c], Takashi Inui [a,*]

[a] Laboratory of Protein Sciences, Graduate School of Life and Environmental Sciences, Osaka Prefecture University, 1-1 Gakuen-cho, Naka-ku, Sakai, Osaka 599-8531, Japan
[b] Research and Utilization Division, Japan Synchrotron Radiation Research Institute, 1-1-1 Koto, Sayo, Hyogo 679-5198, Japan
[c] Laboratory of Biophysical Chemistry, Graduate School of Pharmaceutical Sciences, Osaka University, 1-6 Yamadaoka, Suita, Osaka 565-0871, Japan
[d] Department of Molecular Behavioral Biology, Osaka Bioscience Institute, 6-2-4 Furuedai, Suita, Osaka 565-0874, Japan

ARTICLE INFO

*Article history:*
Received 1 May 2009
Received in revised form 2 October 2009
Accepted 9 October 2009
Available online 13 October 2009

*Keywords:*
Conformational change
Structural flexibility
Ligand binding
SAXS
NMR

ABSTRACT

Lipocalin-type prostaglandin D synthase (L-PGDS) acts as both a $PGD_2$ synthase and an extracellular transporter for small lipophilic molecules. From a series of biochemical studies, it has been found that L-PGDS has an ability to bind a variety of lipophilic ligands such as biliverdin, bilirubin and retinoids *in vitro*. Therefore, we considered that it is necessary to clarify the molecular structure of L-PGDS upon binding ligand in order to understand the physiological relevance of L-PGDS as a transporter protein. We investigated a molecular structure of L-PGDS/biliverdin complex by small-angle X-ray scattering (SAXS) and multi-dimensional NMR measurements, and characterized the binding mechanism in detail. SAXS measurements revealed that L-PGDS has a globular shape and becomes compact by 1.3 Å in radius of gyration on binding biliverdin. NMR experiments revealed that L-PGDS possessed an eight-stranded antiparallel β-barrel forming a central cavity. Upon the titration with biliverdin, some cross-peaks for residues surrounding the cavity and EF-loop and H2-helix above the β-barrel shifted, and the intensity of other cross-peaks decreased with signal broadenings in $^{1}H-^{15}N$ heteronuclear single quantum coherence spectra. These results demonstrate that L-PGDS holds biliverdin within the β-barrel, and the conformation of the loop regions above the β-barrel changes upon binding biliverdin. Through such a conformational change, the whole molecule of L-PGDS becomes compact.



## 1. Introduction

Lipocalin-type prostaglandin (PG) D synthase (L-PGDS, prostaglandin-$H_2$ D-isomerase, EC 5.3.99.2) is the key enzyme being responsible for the formation of $PGD_2$ from $PGH_2$ which is a common precursor of all prostanoids (Urade and Eguchi, 2002). $PGD_2$ plays a role as a neuromodulator in the central nervous system, where it induces sleep and regulates body temperature, luteinizing hormone release and pain responses (Urade and Hayaishi, 2000a). In the peripheral tissues, $PGD_2$ induces vasodilation and bronchoconstriction (Alving et al., 1991; Dumitrascu, 1996) and acts as a mediator of allergy and inflammatory responses (Matsuoka et al., 2000; Urade and Hayaishi, 2000b). L-PGDS was found to be a β-trace protein which is secreted into cerebrospinal fluid (CSF) from the leptomeninges and arachnoid membrane (Urade et al., 1993), and is the second most abundant protein constituent in human CSF (Hoffmann et al., 1993; Kuruvilla et al., 1991).

L-PGDS is also known as a member of the lipocalin superfamily which is composed of various secretory lipophilic ligand transporter proteins such as β-lactoglobulin, retinoic acid binding protein, odorant-binding protein, apolipoprotein D, and tear lipocalin (Breustedt et al., 2005; Eichinger et al., 2007; Flower et al., 2000; Hajjar et al., 2006; Pattanayek and Newcomer, 1999). The lipocalin proteins have a highly symmetrical all-β structure dominated by a single eight-stranded antiparallel β-sheet closed back on itself to form a continuously hydrogen-bonded β-barrel (Cowan et al., 1990; Ganforina et al., 2000). This β-barrel commonly encloses a ligand binding site composed of both an internal cavity and an external loop scaffold (Flower et al., 2000). A number of biochemical studies showed a strong possibility of usage of lipocalins for storage or transport of the physiologically important lipophilic ligands (Flower, 1996; Pervaiz and Brew, 1987). In the case of L-PGDS, a series of our studies showed that it could bind a large variety of lipophilic ligands, such as retinoids, biliverdin, bilirubin, thyroid hormones, gangliosides and amyloid-β peptides *in vitro* (Beuckmann et al., 1999; Inui et al., 1999; Kanekiyo et al., 2007; Mohri et al., 2006; Tanaka et al., 1997). Thus, we defined such a feature as 'broad ligand selectivity' (Inui et al., 2003). We also re-

* Corresponding author. Fax: +81 72 254 9474.
*E-mail address:* inuit@bioinfo.osakafu-u.ac.jp (T. Inui).

1047-8477/$ - see front matter © 2009 Elsevier Inc. All rights reserved.
doi:10.1016/j.jsb.2009.10.005

ported the molecular structure of C89A/C186A-substituted L-PGDS, which is lacking the native disulfide bond, determined by NMR (Shimamoto et al., 2007). In that study, it was revealed that C89A/C186A-substituted L-PGDS had a typical lipocalin fold, which consists of an eight-stranded antiparallel β-barrel and a long α-helix associated with the outer surface of the barrel, and the interior of the barrel formed a hydrophobic cavity. From characterization of unfolding process of L-PGDS, we showed that denaturant-induced unfolding of L-PGDS follows a 4-state pathway including an activity-enhanced state and an inactive intermediate state (Inui et al., 2003). Further, under an acidic condition (pH 4.0), the thermal unfolding of L-PGDS was a completely reversible process, and we proposed a 3-state unfolding through an intermediate state (Iida et al., 2008). Most recently, small-angle X-ray scattering (SAXS) measurements revealed that L-PGDS becomes compact upon binding a lipophilic ligand at pH 8.0, at which the maximum enzymatic activity is observed (Inoue et al., 2009). Through this work, the structural flexibility of L-PGDS molecule was directly demonstrated and it was also suggested that such a structural flexibility was related to the broad ligand selectivity.

In terms of clinical importance, some reports have indicated that the concentration of L-PGDS in CSF is a useful clinical marker to diagnose neurological diseases. The concentration of L-PGDS increased in CSF of patients in spinal canal stenosis (Tumani et al., 1998), while it was significantly lower in patients with schizophrenia (Harrington et al., 1993), brain tumor (Saso et al., 1998), bacterial meningitis (Tumani et al., 1998), and normal pressure hydrocephalus (Mase et al., 2003). L-PGDS was also proposed to be a diagnostic marker for *N*-glycosylation defects in the central nervous system (Grunewald et al., 1999). In addition, we previously found that the concentration of L-PGDS in CSF increased transiently in patients with aneurysmal subarachnoid hemorrhage (SAH) in its acute stage and the L-PGDS purified from the CSF of SAH patients bound bile pigments, the metabolites of hemoglobin (Inui et al., 2002; Mase et al., 1999). These reports of ours suggest that L-PGDS physiologically plays an important role in CSF of patients with SAH. Therefore, we considered that in order to understand the physiological relevance of L-PGDS in CSF it is necessary to clarify the molecular structure of L-PGDS upon binding bile pigments.

Although a number of studies have been done so far, the detailed mechanism of ligand binding on L-PGDS remains elusive, because of insufficient data from structural studies on the protein molecule itself. In the present study, therefore, we performed SAXS and multi-dimensional NMR measurements in order to elucidate the molecular structure and conformational changes of L-PGDS upon binding biliverdin, a lipophilic ligand. The combination of SAXS and NMR measurement is very useful not only for resolving protein structure but also characterizing conformational dynamics and changes in the size and the overall shape of proteins under solution conditions. These structural studies on the L-PGDS molecule will lead to detailed understanding for the mechanism of broad ligand selectivity as well as to predictive clinical applications of L-PGDS for SAH, especially for the improvement of prognosis. On the view point of physiological importance, biliverdin was chosen as a representative ligand, because it was one of the bile pigments. Based on results from these experiments, we propose that biliverdin enters the large cavity of the β-barrel, which triggers conformational changes that induce global compaction of the L-PGDS molecule. These conformational changes may induce proper interactions between the protein and the ligand, and consequently the ligand is tightly held inside the L-PGDS molecule. From all structural information, it was considered that L-PGDS molecule was structurally flexible, and thus the specific character of L-PGDS, i.e., broad ligand selectivity, may be attributable to its flexibility.

## 2. Materials and methods

### 2.1. Chemicals

Thrombin and biliverdin were purchased from Sigma Chemical Co. (St. Louis, MO). All other chemicals were in the analytical grade.

### 2.2. Expression of recombinant mouse C65A-substituted L-PGDS

In all experiments, a mouse Δ1-24-C65A-substituted L-PGDS mutant, which preserves a disulfide bond between Cys89 and Cys186, was used.

The mouse Δ1-24-C65A-substituted L-PGDS mutant, in which the N-terminal signal peptide sequence was removed, was expressed as a glutathione *S*-transferase fusion protein in *Escherichia coli* BL21 (DE3) (TOYOBO, Tokyo, Japan) as described previously (Inui et al., 1999). The fusion protein was bound to glutathione–Sepharose 4B (GE Healthcare Bio-Sciences, Little Chalfont, UK) and incubated with thrombin (Sigma Chemical Co., St. Louis, MO, USA) (100 U per 100 μl) to release the L-PGDS. This mutant protein possessing an intrinsic disulfide bond is more stable than the mouse C89A/C186A-substituted recombinant protein used previously (Inui et al., 2003). The recombinant protein was further purified by using size-exclusion chromatography as described previously (Inui et al., 2003). Then, the purified protein was dialyzed against 20 mM sodium acetate (pH 4.0). The protein concentration was determined spectroscopically by using the molar extinction coefficient at 280 nm, $E_{280\mathrm{nm}}$ = 23,000 $M^{-1}$ $cm^{-1}$.

### 2.3. Fluorescence quenching assay

Biliverdin was dissolved in dimethyl sulfoxide (DMSO) to give a 2 mM stock solution. The concentrations were determined spectroscopically based on their respective molar absorption coefficients of $E_{377\mathrm{nm}}$ in methanol for biliverdin = 51,500 $M^{-1}$ $cm^{-1}$ (McPhee et al., 1996). Various concentrations of biliverdin were added to L-PGDS, in 20 mM sodium acetate for pH 4.0 to give a final L-PGDS concentration of 1.5 μM. After incubation at 25 °C for 30 min, the intrinsic tryptophan fluorescence was measured as described previously (Inui et al., 2003). The dissociation constant ($K_d$) and the molar ratio ($n$) for binding between biliverdin and L-PGDS was calculated by the method described earlier (Cogan et al., 1976).

### 2.4. Small-angle X-ray scattering measurements

Small-angle X-ray scattering (SAXS) data collection was carried out at BL40B2, which is a bending magnet beamline in the SPring-8 synchrotron radiation facility (Hyogo, Japan). The X-ray wavelength was tuned to 1.0 Å, the sample-to-detector distance was set to 1050 mm, and the X-ray flux at the sample was estimated as $4 \times 10^{10}$ photons/s. All the experiments were performed at 25 °C. Data were collected using an R-AXIS IV$^{++}$ system (RIGAKU, Tokyo, Japan) as a detector (Inoue et al., 2004). A sample cell with a thickness of 3.0 mm was used to maximize scattering of X-ray. The windows of the cell were made of 0.02 mm thick quartz plates. The exposure times for each measurement were from 10 s to 20 s depending on the concentration of the sample, long enough to obtain a sufficient signal-to-noise ratio and but short enough to avoid the radiation damage. In order to check for the radiation damage, we routinely compared the scattering curves with several different exposure times and confirmed that no aggregates of the protein were formed by the radiation damage in 10–20 s. To avoid systematic errors, we measured sample and buffer solutions alternately. For SAXS measurements, L-PGDS was mixed with biliverdin in a 1:3 M concentration ratio. After 1 h of stirring, in order to remove DMSO and free

biliverdin from the solvent and aggregates, the mixture was applied to a PD10 column (GE Healthcare Bio-Sciences); and only the fractions containing complexes were gathered. Data were recorded for protein concentrations of 2.5 mg $mL^{-1}$, 5.0 mg $mL^{-1}$, 8.0 mg $mL^{-1}$, and 12.0 mg $mL^{-1}$. In each series of experiments, SAXS profiles of ovalbumin ($Mr$ = 45,000, Sigma) and lysozyme ($Mr$ = 14,300, SEIKAGAKU CORPORATION, Tokyo, Japan) were collected as a reference for molecular mass determination.

Two-dimensionally recorded scattering patterns were transformed to a one-dimensional profile by circular averaging. Contributions to scattering intensities from the solvent were eliminated from the raw data by subtracting the intensity curve obtained for the buffer solution. Scattering profiles in the small-angle region were analyzed by Guinier's approximation for monodispersive systems (Guinier and Fournet, 1955): the scattering intensity ($I(S,C)$) as a function of the reciprocal vector ($S$) and protein concentration ($C$), is expressed by the forward scattering intensity ($I(0,C)$) and the radius of gyration ($R_g(C)$) as.

$$I(S,C) = I(0,C)\exp\left[-\frac{4}{3}\pi^2 \times R_g(C)^2 S^2\right],$$

$$S = \frac{2\sin\theta}{\lambda},$$

where $2\theta$ is the scattering angle relative to the incident beam and $\lambda$ is the X-ray wavelength. The reciprocal vector ($S$) was calibrated by meridional reflections from chicken tendon collagen. In order to eliminate interparticle interference, we made measurements at four different protein concentrations and then extrapolated these data points to zero protein concentration. Intraparticle distance distribution functions ($P(r)$), were calculated from the experimental scattering data using the GNOM package (Svergun, 1992). The values of the maximum diameters of the particle ($D_{max}$) were determined empirically by examining the quality of the fit to the experimental data for a range of $D_{max}$ values. Assuming a partial specific volume of 0.73 $cm^3\ g^{-1}$ for soluble proteins, the molecular mass of a protein is determined by using $I(0,C=0)$ of a reference protein with a known molecular mass.

### 2.5. Ab initio modeling

*Ab initio* model structures of L-PGDS was calculated using *ab initio* structure determination program GASBOR package (Svergun et al., 2001) to scattering profiles weighted by $S^{-4}$ to ensure Porod's law in $S < 0.015$ $Å^{-1}$. The programs minimized the discrepancy between the experimental $I_{exp}(S)$ and calculated $I_{model}(S)$ profiles by keeping a compactly interconnected configuration of dummy particles. Discrepancies were examined with the $\chi^2$ values (Fukuhara et al., 2004; Svergun, 1999) defined as

$$\chi^2 = \frac{1}{N-1}\sum\left\{\frac{I_{exp}(S_j) - K_{model}I_{model}(S_j)}{\sigma(S_j)}\right\}^2,$$

where $N$ is the number of experimental datum points, $K_{model}$ is a scaling factor, and $\sigma(S_j)$ is the statistical error of $I_{exp}(S_j)$ at the scattering vector $S_j$ (Svergun et al., 2001). The modeling calculations were repeated until the $\chi^2$ of each model became less than 2.0. The 10 models having almost the same overall structures were superimposed and averaged with SUPCOMB (Kozin and Svergun, 2001).

### 2.6. NMR measurements

#### 2.6.1. Signal assignments for L-PGDS in the absence of biliverdin

Isotopically labeled C65A-substituted L-PGDS was prepared as reported previously (Inui et al., 2003) except that *E. coli* cells were cultured in M9 minimal medium containing $^{15}NH_4Cl$ (1 g $L^{-1}$) and/or $^{13}C$ glucose (5 g $L^{-1}$) as sole nitrogen and carbon sources. At first, we tried to measure $^1H$–$^{15}N$ heteronuclear single quantum coherence (HSQC) spectrum of C65A-substituted L-PGDS at pH 6.5. However, most of the signals were broadened and the signals of the residues at EF-loop and H2-helix could not be assigned (data not shown). This might be due to the faster exchange of amide protons of L-PGDS with water (Dempsey, 2001; Wüthrich, 1986) and/or the conformational exchange of EF-loop and H2-helix at pH 6.5. In order to improve the spectral quality we changed the condition of NMR measurement from a neutral pH to an acidic pH. The far-UV circular dichroism (CD) spectrum of C65A-substituted L-PGDS at pH 4.0 was almost the same as that at pH 6.5, indicating that there is no significant structural difference in overall secondary structures of C65A-substituted L-PGDS between pH 4.0 and pH 6.5 (Supplementary Fig. 1). Then, the NMR samples were prepared in 20 mM sodium acetate of $D_2O$ or 90% $H_2O$/10% $D_2O$ mixture at pH 4.0. The protein concentration was adjusted to approximately 0.5 mM in 5-mm microcell NMR tube (Shigemi Inc., Tokyo, Japan) for all NMR experiments. All two- and three-dimensional NMR experiments were performed at 25 °C on a Varian INOVA500 spectrometer or a Varian INOVA600 spectrometer equipped with a triple-resonance ($^1H$, $^{13}C$, and $^{15}N$) probe and shielded $z$-gradient. The pulsed-field gradient techniques with a WATERGATE (Piotto et al., 1992) were utilized in all $H_2O$ experiments for the solvent suppression. Transmitter frequencies for $^1H$, $^{15}N$, $^{13}C\alpha$, aliphatic $^{13}C$, and aromatic $^{13}C$ were typically set to 4.77, 119.0, 60.8, 43.0, and 110.0 ppm, respectively. Sodium 2,2-dimethyl-2-silapentane-5-sulfonate (DSS) was used as an external reference of $^1H$ chemical shifts. $^{15}N$ and $^{13}C$ chemical shifts were indirectly calibrated from each gyromagnetic ratio (Wishart et al., 1995). Backbone and side-chain assignments of L-PGDS were obtained from 2D $^1H$–$^{15}N$ HSQC, 2D $^{13}C$–$^1H$ HSQC, 2D $^{13}C$–$^1H$ (HB)CB(CGCD)HD (Yamazaki et al., 1993), 3D HNCACB, 3D CBCA(CO)NH, 3D HBHA(CBCACO)NH, and 3D HCCH-TOCSY spectroscopy (Bax et al., 1994; Kay, 1995). Almost complete signal assignments were achieved for backbone and side-chain $^1H$, $^{13}C$, and $^{15}N$ resonances of L-PGDS at pH 4.0. NMR distance restraints were derived from 3D $^{15}N$-edited NOESY (100 ms mixing time) and 3D $^{13}C$-edited NOESY (100 ms mixing time) experiments (Bax et al., 1994; Kay, 1995), as well as from the 2D NOESY (100 ms mixing time) experiment acquired. All the NMR spectra were processed and analyzed using NMRPipe (Delaglio et al., 1995) and Sparky (Goddard, T.D., and Kneller, D.G., SPARKY 3, University of California, San Francisco).

#### 2.6.2. Structure calculation

Nuclear Overhauser effect (NOE) restrains were classified into four categories: strong, medium, weak, and very weak corresponding to the distance restraints of 1.8–2.8 Å, 1.8–3.4 Å, 1.8–4.2 Å, and 1.8–5.0 Å, respectively. A total of 1479 NOE restraints were employed for this structure calculation, including 492 intraresidues, 481 sequential, and 181 medium-range ($i-i+2$, $i-i+3$, $i-i+4$) and 325 long-range restraints. In addition, the 202 $\phi$ and $\psi$ torsion angle restraints were evaluated from backbone chemical shifts of $^{15}N$, H$\alpha$, $^{13}C\alpha$, and $^{13}C\beta$ using the program TALOS (Cornilescu et al., 1999). The structure calculation was performed with a simulated annealing algorithm in the program CNS 1.2 (Brunger, 2007). Finally, the structural ensemble comprised 10 lowest energy structures were selected and analyzed by using the programs MOLMOL (Koradi et al., 1996) and PROCHECK 3.54 (Laskowski et al., 1996). Graphical representations were prepared using PyMOL (W.L. DeLano, http://www.pymol.org). Chemical shift assignments and distance constraints for the free form of L-PGDS have been deposited in the Biological Magnetic Resonance Data Bank (http://www.bmrb.wisc.edu) with an accession number 11062. Atomic coordinates and structure factors for solution structure of

L-PGDS possessing an intrinsic disulfide bond have been deposited in the Protein Data Bank (http://www.rcsb.org) with PDB ID code 2RQ0.

*2.6.3. Measurements of the chemical shift perturbations upon binding of biliverdin*

Titration with biliverdin was monitored by an NMR titration of $^{15}$N-labeled L-PGDS with unlabeled biliverdin using $^{1}$H–$^{15}$N HSQC experiments. Biliverdin was added to 0.5 mM L-PGDS to a final concentration of 0.3 mM. The composite chemical shift differences ($\Delta\delta_{tot}$) were calculated as.

$$\Delta\delta_{tot} = \sqrt{(\Delta\delta_{HN} \times W_{HN})^2 + (\Delta\delta_{N} \times W_{N})^2},$$

where $\Delta\delta_{HN}$ and $\Delta\delta_{N}$ are the chemical shift changes of $^{1}$H and $^{15}$N, respectively. The weighting factors used were $W_{HN} = 1$ and $W_{N} = 0.2$.

## 3. Results

### 3.1. Binding affinity of biliverdin for L-PGDS

At first, to investigate the binding affinity of biliverdin to L-PGDS, we measured the fluorescence quenching of intrinsic tryptophan residues of L-PGDS with various concentrations of biliverdin at pH 4.0. Mouse L-PGDS contains two tryptophan residues at positions 43 and 54, and both tryptophan residues contributed to the fluorescence quenching of L-PGDS by the ligand binding (Inui et al., 2003). L-PGDS showed fluorescence quenching in a concentration-dependent manner with biliverdin (Fig. 1). The fluorescence intensity decreased to less than 10% of that of L-PGDS itself in the presence of 5 μM biliverdin. From the quenching curve, the $K_d$ value of biliverdin for L-PGDS was calculated to be 590 ± 72 nM with a binding stoichiometry of 1:1. This result demonstrates that L-PGDS exhibited a high binding affinity for biliverdin under an acidic condition.

### 3.2. SAXS analysis

SAXS is a powerful technique for directly obtaining and characterizing the size, overall shape, and compactness of molecules under solution conditions, and thus is particularly useful for studying systems in which a structural or a conformational change takes place (Guinier and Fournet, 1955). The scattering curves of L-PGDS and L-PGDS/biliverdin showed a large central peak at a reciprocal vector ($S$) < 0.033 Å$^{-1}$, a second peak at $S$ = 0.044 Å$^{-1}$, and a small maximum at $S$ = 0.078 Å$^{-1}$ (Fig. 2). The scattering intensity curves revealed that L-PGDS had a globular shape both in the presence or absence of biliverdin. The binding of biliverdin to L-PGDS caused clear changes in the scattering curve in the small-angle region ($S$ < 0.02 Å$^{-1}$, Fig. 2). By analyzing scattering curves very carefully, a small but significant peak shift towards the higher $S$ region was found for the second peak ($S$ = 0.044 Å$^{-1}$, Fig. 2), and also for the third peak ($S$ = 0.078 Å$^{-1}$, Fig. 2). All such changes imply that the L-PGDS molecule has become compact after binding the ligand. The apparent radius of gyration ($R_g(C)$) and the normalized forward scattering intensity ($I(0,C)$) were calculated from the slope and intercept, respectively, of the linear regression lines in the Guinier plot. A Guinier plot of the scattering data showed a linear correlation between ln ($I(S)/C$) and $S^2$ at low values of $S$, and the slope of this plot provided $R_g$ of the molecules. The Guinier plot at different concentrations of L-PGDS (Fig. 3A) showed a linear regression line without significant upward curvature even at the low $S^2$ region, indicating that the sample solution was mono-dispersed without aggregation even at the highest concentration (12.0 mg mL$^{-1}$). The Guinier plot of the SAXS data obtained from L-PGDS/biliverdin complex also showed the same feature as that of L-PGDS (data not shown). When the calculated $R_g(C)^2$ and $I(0,C)/C$ values were plotted as a function of the protein concentration (Figs. 3B and C), the values obtained from L-PGDS and L-PGDS/biliverdin showed a linear and negative concentration-dependency. The slope of the plot (Fig. 3B) corresponds to the second virial coefficient, and the negative slope indicated the repulsive interactions between L-PGDS molecules.

From the linear extrapolations of $R_g(C)^2$ to infinite dilution, which eliminated interparticle interferences, $R_g(0)$ values of L-PGDS and L-PGDS/biliverdin were evaluated to be 19.2 ± 0.26 and 17.9 ± 0.20 Å, respectively (Table 1). Thus, L-PGDS became compact by approximately 1.3 Å in radius after binding biliverdin. The molecular masses of L-PGDS and L-PGDS/biliverdin were estimated to be 2.0 × 10$^4$ and 2.1 × 10$^4$ Da, respectively, by the linear relation between the forward scattering intensity and the molecular mass of the protein (Table 1). The estimated molecular mass of L-PGDS was in good agreement with that of L-PGDS calculated from its amino acid sequence (1.9 × 10$^4$ Da). The estimated molecular mass of L-PGDS/biliverdin was larger than that of L-PGDS due to the

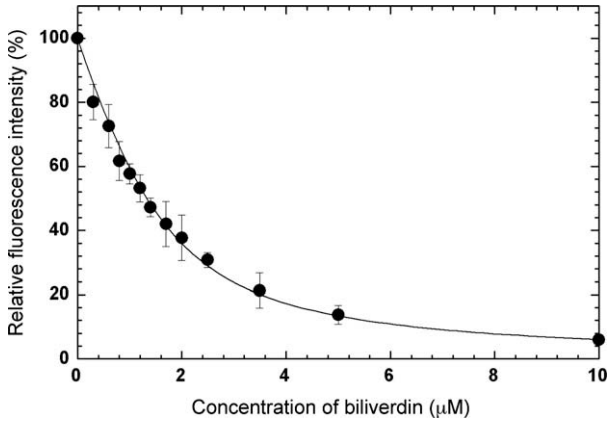


**Fig. 1.** Fluorescence quenching of tryptophan residues by binding of biliverdin. The concentration of protein was adjusted to 1.5 μM. The relative fluorescence intensities of L-PGDS in the presence of various concentrations of biliverdin were obtained. Data are expressed as the mean ± SD of 3 independent measurements.

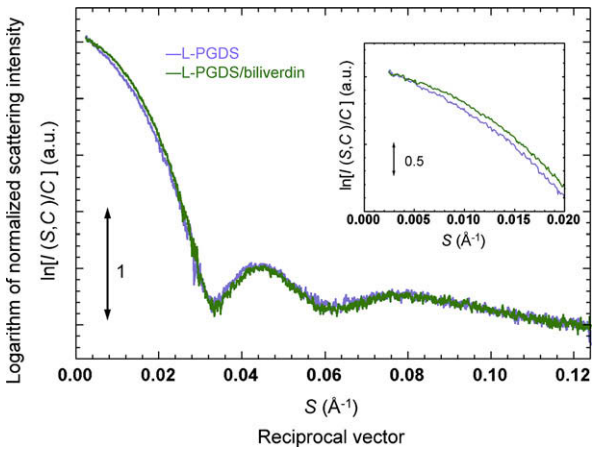


**Fig. 2.** SAXS profiles of L-PGDS and L-PGDS/biliverdin complex. SAXS profiles of L-PGDS (blue line) and L-PGDS/biliverdin (green line) are shown. These profiles were obtained by extrapolating of all data at different concentrations (12, 8, 5, and 2.5 mg mL$^{-1}$) to the zero concentration. The logarithm of scattering intensity is shown as a function of reciprocal vector ($S$). Inset shows the logarithm of scattering intensity in the small $S$ region.

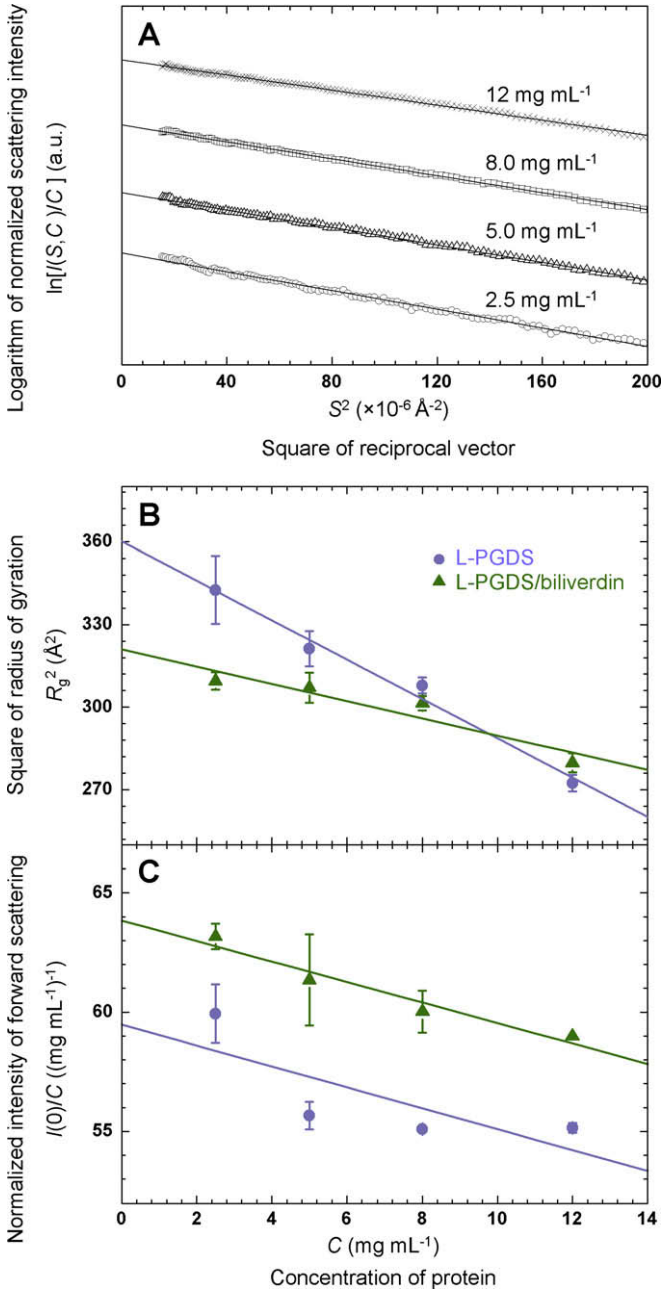


**Fig. 3.** Examples of analysis of data obtained from SAXS experiments. (A) Example of Guinier plots. The values of the $R_g$ and $I(0,C)$ were determined by the Guinier approximation from the low $S$ regions ($2\pi SR_g < 1.3$) of the scattering profiles. Logarithms of intensities plotted against squared scattering vector length of L-PGDS at concentrations of 2.5 mg mL$^{-1}$ (○), 5.0 mg mL$^{-1}$ (△), 8.0 mg mL$^{-1}$ (□), and 12.0 mg mL$^{-1}$ (×) are shown. They have been shifted along the ordinate for clarity. Concentration dependence of $R_g^2$ (B) and $I(0,C)/C$ (C) of L-PGDS (blue line) and L-PGDS/biliverdin (green line) is shown. Data are expressed as the mean ± SD of 3 independent experiments.

**Table 1**
Binding affinity of L-PGDS for biliverdin, and changes in $R_g$ and molecular mass of L-PGDS induced by binding of biliverdin.

| | $K_d$ for biliverdin (nM) | $R_g$ (0) (Å) | $I(0,0)$ | Molecular mass (Da) |
|---|---|---|---|---|
| L-PGDS | – | 19.2 ± 0.26 | 59.5 ± 2.00 | $2.0 \times 10^4$ |
| L-PGDS/ biliverdin | 590 ± 72 | 17.9 ± 0.20 | 63.8 ± 0.56 | $2.1 \times 10^4$ |

binding of biliverdin ($Mr$ = 582.6). The slope of the concentration-dependent curves of $R_g(C)^2$ and $I(0,C)/C$ was slightly different for each sample. These results indicated that interparticle interferences in solution were different between the presence and absence of biliverdin.

The intraparticle distance distribution functions, $P(r)$ were calculated as the inverse Fourier transform of the scattering curves of L-PGDS and L-PGDS/biliverdin (Fig. 4). The profiles of $P(r)$ of L-PGDS showed a single peak at 23 Å and were very similar in the presence and absence of biliverdin. The $P(r)$ functions indicate that L-PGDS remains essentially globular after binding biliverdin. The calculated maximum diameters ($D_{max}$) for the L-PGDS/biliverdin were slightly smaller than that for L-PGDS. Such a tendency towards compaction of L-PGDS upon biliverdin binding was consistent with tendencies in all other data. *Ab initio* models of L-PGDS and L-PGDS/biliverdin were calculated using GASBOR package (Svergun et al., 2001). The models resulting from ten individual GASBOR runs were filtered and averaged (DAMAVER (Volkov and Svergun, 2003)) to obtain the most likely molecular model. *Ab initio* models of L-PGDS and L-PGDS/biliverdin showed that the overall structure of the molecule was globular in shape and that the L-PGDS molecule complexed with biliverdin was smaller than that of L-PGDS (Fig. 4 *inset*). The compact packing of L-PGDS upon biliverdin binding revealed by SAXS prompted us to elucidate detailed structure of the L-PGDS/biliverdin complex, and also the binding mode of biliverdin to L-PGDS. Thus, we next measured the multi-dimensional NMR of L-PGDS and L-PGDS/biliverdin complexes.

### 3.3. NMR solution structure of L-PGDS

The solution structure of C65A-substituted L-PGDS, which possesses an intrinsic disulfide bond, was determined by means of multi-dimensional NMR and simulated annealing. Through a series of NMR experiments, almost complete assignments for $^1$H, $^{13}$C and $^{15}$N signals were done. Structural statistics are shown in Table 2. The final structural ensemble comprised 10 structures of the lowest total energy that are superimposed in Fig. 5A. These had no distance restraint violations greater than 0.5 Å and no torsion angle restraint violations above 5 Å. Ramachandran $\phi-\psi$ plots for the ensemble of 10 structures indicate that 83.9% of the non-glycine and non-proline residues were found in the most favored regions,

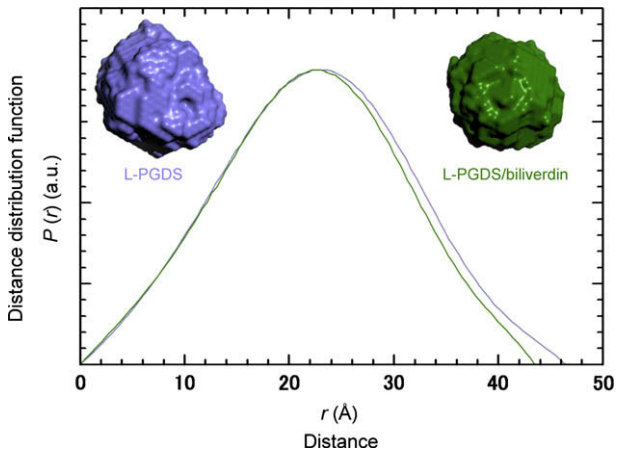


**Fig. 4.** Distance distribution functions ($P(r)$) and *ab initio* models of L-PGDS, and L-PGDS/biliverdin. The $P(r)$ of L-PGDS (blue line) and L-PGDS/biliverdin (green line) are shown. The curves were calculated from the SAXS profiles of each protein. Inset shows *ab initio* models of L-PGDS (blue) and L-PGDS/biliverdin (green). Each *ab initio* model was calculated from a $P(r)$ function by using GASBOR.

**Table 2**
Data collection and refinement statistics.

| | |
|---|---|
| No. of restraints | |
| NOE distance restraints | 1479 |
| Intraresidue | 492 |
| Sequential | 481 |
| Medium range | 181 |
| Long range | 325 |
| Dihedral angle restraints | 202 |
| Deviations from idealized covalent geometry | |
| Bonds (Å) | 0.0034 ± 0.0000 |
| Angle (°) | 0.3784 ± 0.0026 |
| Impropers (°) | 0.2937 ± 0.0050 |
| Mean coordinate RMSD from mean structure[a] (Å) | |
| Overall structure (residue 30–189) | |
| Backbone heavy atoms | 1.19 ± 0.14 |
| All heavy atoms | 1.88 ± 0.13 |
| Secondary elements | |
| Backbone heavy atoms | 0.48 ± 0.08 |
| All heavy atoms | 1.10 ± 0.08 |
| Ramachandran plot analysis (%) | |
| Residues in most favored regions | 99.2 |
| Most favored regions | 83.9 |
| Additionally allowed regions | 12.8 |
| Generously allowed regions | 2.6 |
| Residues in disallowed regions | 0.8 |

[a] Calculated from the final structural ensemble (10 structures).

12.8% were found in the additional allowed regions, and 2.6% were found in the generously allowed regions. Several residues at the N terminus are found around the border of the disallowed region probably due to the lack of experimental information of the $\phi-\psi$ angle values (Bertini et al., 2003). The superposition of the backbone atoms clearly shows that the calculated structures were well converged, except for the first eight residues at the N terminus and the last three residues at the C terminus (Fig. 5A). The overall average root mean square deviation (RMSD) value was 1.19 ± 0.14 Å for the mean structure with backbone heavy atoms only, and 1.88 ± 0.13 Å for those with all heavy atoms including side chains of L-PGDS (residues 30–189). The average RMSD values for backbone heavy atoms was 0.48 ± 0.08 Å, and those for all heavy atoms in the regular secondary structure elements (residues 41–48, 65–70, 76–83, 90–97, 105–107, 117–121, 129–133, 144–149, 158–167) was 1.10 ± 0.08 Å.

A ribbon diagram of a representative lowest energy NMR structure of L-PGDS is shown in Fig. 5B. L-PGDS possessed an eight-stranded antiparallel β-barrel which formed a central cavity at pH 4.0. The cavity opens to one end of the β-barrel, where a short helix and three loops, CD-loop, EF-loop, and GH-loop, connect neighboring β-strands in a pairwise fashion. All these structural features are typical and well conserved for the lipocalin superfamily, and the same is true for L-PGDS. Secondary structural elements of L-PGDS were comprised of nine β-strands (A, residues 41–50; B, 64–71; C, 77–84; D, 89–98; E, 104–109; F, 114–123; G, 128–135; H, 143–150; I, 177–178) plus a short $3_{10}$-helix (H1, 35–40) and two α-helices (H2, 53–60; H3, 156–171) (Fig. 5B). L-PGDS has three cysteine residues, Cys65, Cys89, and Cys186, and two of these cysteine residues, Cys89 and Cys186, form a disulfide bridge, which is also highly conserved among most lipocalins. The Trp43 residue is located at the bottom of the hydrophobic cavity, whereas the Trp54 residue is located in the H2-helix. We previously reported that the molecular structure of C89A/C186A-substituted L-PGDS determined by NMR exhibited the typical lipocalin fold at pH 6.5 and showed that C89A/C186A-substituted L-PGDS possessed a short $3_{10}$-helix (residues 56–60) between the A and B strands (Shimamoto et al., 2007). In the present study, however, a full turn of α-helix was exhibited in C65A-substituted L-PGDS at the residues of 53–60 (Supplementary Fig. 2). We think it demonstrates that the signal assignments of the backbone and side-chain $^{1}H$, $^{13}C$, and $^{15}N$ resonances for C65A-substituted L-PGDS were done much better than those for C89A/C186A-substituted L-PGDS. Further, we compared the structure of C65A-substituted L-PGDS with that of C89A/C186A-substituted L-PGDS to investigate the importance of an intrinsic disulfide bond (Supplementary Fig. 2). The mean structure was obtained by averaging coordinates of final 10 structures for both proteins. The difference of backbone RMSD for the overall structure of mean structure between two proteins (residues 30–186) was 1.054 ± 0.002 Å. This result revealed that the overall structure of C65A-substituted L-PGDS was very similar to that of C89A/C186A-substituted L-PGDS and such a structural similarity suggested that the intrinsic disulfide bond did not affect the overall structure of L-PGDS. In other words, it was suggested that the overall structure of C89A/C186A-substituted L-PGDS was very similar to that of wild-type L-PGDS as well as that of C65A-substituted L-PGDS.

### 3.4. Chemical shift perturbations of L-PGDS induced by the binding of biliverdin

We monitored titration with biliverdin using two-dimensional $^{1}H-^{15}N$ HSQC spectra. The concentration of L-PGDS was fixed at

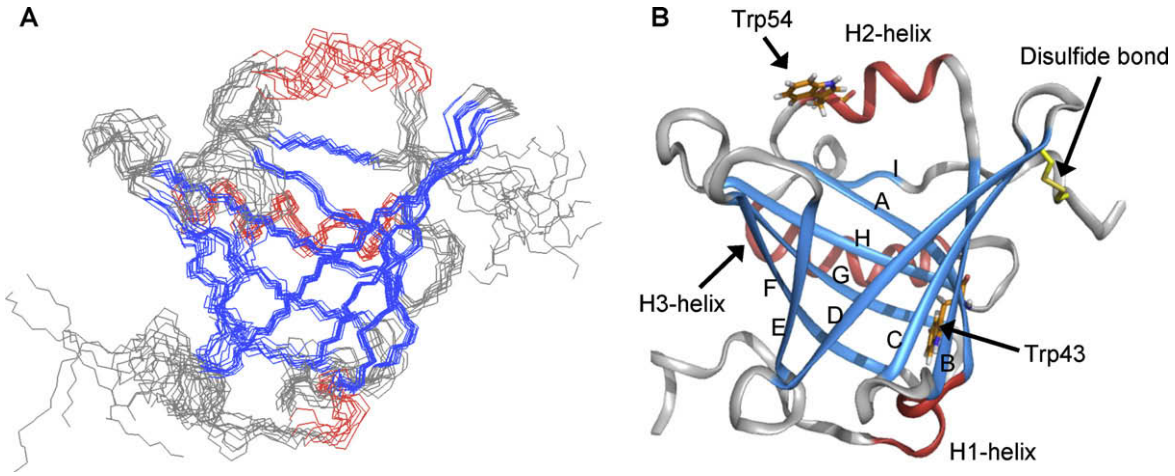


**Fig. 5.** Solution structure of C65A-substituted L-PGDS. (A) The final structural ensemble comprised 10 structures with the lowest total energy. (B) Ribbon representation showing the typical lipocalin fold of L-PGDS with disulfide bond in yellow and tryptophan residues in orange, respectively. The secondary structure elements are labeled and colored red and blue for helices and β-strands, respectively.

0.5 mM, and that of biliverdin was varied from 0 to 0.3 mM. The $^{1}H$–$^{15}N$ HSQC spectra were recorded at the respective concentration of biliverdin. As the concentration of biliverdin increased, some cross-peaks shifted and intensity of some other peaks decreased with signal broadening (Fig. 6A). To allow quantification of the observed chemical shift changes, backbone signals of L-PGDS in the complex with 0.3 mM biliverdin were assigned (Supplementary Table 1). Fig. 6B presents the magnitude of the composite $^{1}H$ and $^{15}N$ chemical shift perturbations of the backbone amide protons and nitrogen atoms caused by the binding of biliverdin. It is displayed along the primary sequence. With 0.3 mM biliverdin, 16% of the signals (26 of 167 cross-peaks) showed chemical shift perturbations larger than 0.10 ppm (Fig. 6B). The mapping of these residues ($\Delta\delta_{tot} > 0.10$ ppm) on the solution structure of C65A-substituted L-PGDS revealed that they were located in the C, D, E, F, G, and H strands, EF-loop, and H2-helix (Fig. 7A, residues colored in red). These signal perturbations indicated that the environment of these residues altered upon binding of biliverdin, showing that biliverdin binds within the β-barrel of L-PGDS. Further, 20% of the signals (33 of 167) disappeared on the $^{1}H$–$^{15}N$ HSQC spectrum (Fig. 6B and Supplementary Fig. 3), and these missing residues were surrounding the cavity or located in the H2-helix (Fig. 7A, residues colored in green). From these results, it was concluded that a bound biliverdin was held through contacts with a rather broad area of the inner side of the L-PGDS molecule.

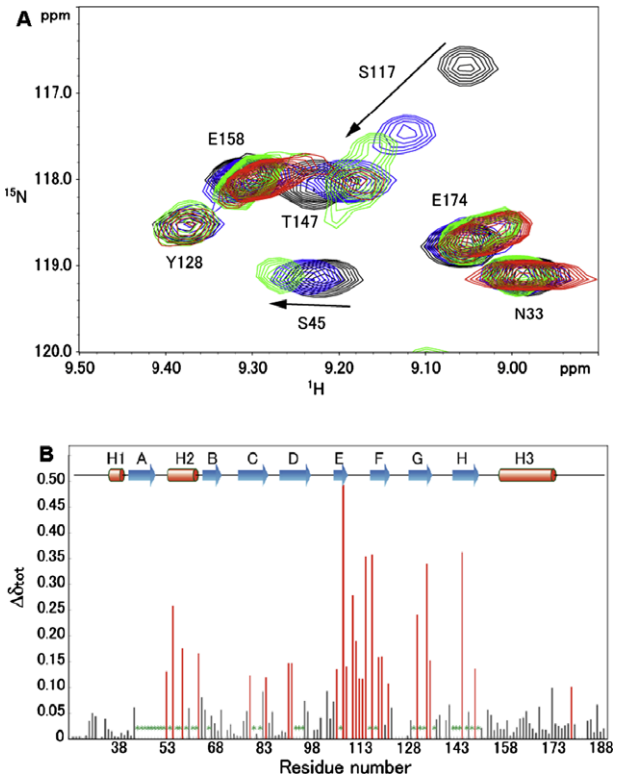


**Fig. 6.** NMR titration of L-PGDS with biliverdin. (A) Representative region of the $^{1}H$-$^{15}N$ HSQC spectra of L-PGDS, showing the superposition of the spectra of L-PGDS (black peaks) and L-PGDS/biliverdin ([L-PGDS] = 0.5 mM and [biliverdin] = 0.05 mM (blue), 0.2 mM (green), and 0.3 mM (red)). (B) Chemical shift perturbations induced by the binding of biliverdin observed on the backbone amide groups of L-PGDS. The composite $^{1}H$ and $^{15}N$ chemical shift perturbations ($\Delta\delta_{tot}$) *versus* the amino acid sequence. The residues with relatively large changes ($\Delta\delta_{tot} > 0.10$ ppm) are represented by red bar. The residues with signals that disappeared upon binding of biliverdin (0.3 mM) are represented by green asterisk.

## 4. Discussion

In this study, the fluorescence quenching assay revealed the high binding affinity of biliverdin to L-PGDS ($K_d$ = 590 nM). The SAXS data revealed that L-PGDS molecule possesses a globular shape and the experimental SAXS profile of L-PGDS is in a good agreement ($\chi$ = 2.7) with the SAXS profile calculated from NMR structure with CRYSOL (Svergun et al., 1995, Supplementary Fig. 4). After binding biliverdin, L-PGDS became compact. The compactness was also clearly suggested in the *ab initio* model structures using GASBOR. The NMR analysis showed the changes in the chemical shift and signal broadenings in a broad area of the β-barrel, the EF-loop and the H2-helix upon the binding of biliverdin. On the other hand, in the absence of biliverdin broad cross-peaks were observed for the residues located in H2-helix on $^{1}H$–$^{15}N$ HSQC spectrum and conformational exchange on a time scale of microseconds to milliseconds was observed for the C-terminal region of the helix by $^{15}N$ relaxation measurements, indicating that H2-helix is originally flexible in solution (Supplementary Fig. 3 and Supplementary Fig. 5).

Combining these results, it is considered that the conformational changes are induced on the EF-loop and the H2-helix causing a compact packing in the entire molecule of L-PGDS after binding biliverdin. Considering all these lines of evidence, we propose a binding mechanism of the lipophilic ligand to L-PGDS (Fig. 8): at the initial step the ligand binds to L-PGDS by hydrophobic interactions, and then some local movements in the molecule, such as in the EF-loop and the H2-helix, induce a compact packing still keeping the global β-barrel structure unchanged. So far, only a few studies on lipocalin family proteins reported conformational changes due to ligand binding. In the case of bovine β-lactoglobulin, NMR spectroscopy revealed that the entrance region of the β-barrel, especially the D strand and the EF and GH-loops, fluctuate upon binding of palmitic acid, suggesting that the β-barrel entrance can change its conformation to allow various conformations of the bound palmitic acid (Konuma et al., 2007). This report supports our results for conformational changes in the loop regions above the β-barrel of L-PGDS. Such a structural flexibility is considered to lead not only to a proper interaction between L-PGDS and the ligand, but also to the ability to bind a variety of ligands, the so-called 'broad ligand selectivity'.

As is shown in Fig. 7A, we found that large chemical shift changes ($\Delta\delta_{tot} > 0.10$ ppm) and the disappearances of signals occurred in residues within the whole region of the β-barrel, EF-loop, and H2-helix of C65A-substituted L-PGDS upon binding of biliverdin. This was totally different from the result of C89A/C186A-substituted L-PGDS bound all-*trans* retinoic acid shown in Fig. 7B: large chemical shift changes ($\Delta\delta_{tot} > 0.08$ ppm) were observed only at the F and G strands and the signals of the residues located in the β-barrel were still observed with all-*trans* retinoic acid (Shimamoto et al., 2007). Therefore, all-*trans* retinoic acid bound on the F and G strands, and the cyclohexene ring of retinoic acid was placed in the smaller hydrophobic pocket located at the lower part of the cavity. Judging from the wide contact area of L-PGDS to ligand, we consider that the bound biliverdin molecule might not be oriented in one direction. Each signal originated from each binding mode could not be distinguished because of the large number of the binding modes and/or the averaging between them by the exchange on the time scale of chemical shift. Therefore, the binding mode for biliverdin could be completely different from that for all-*trans* retinoic acid. This idea is supported also by our most recent study which reported using SAXS measurements that L-PGDS becomes compact upon binding lipophilic ligands at pH 8.0 (Inoue et al., 2009). The calculated values of $R_g$ were 19.4 Å for L-PGDS, 17.8 Å for L-PGDS/biliverdin complex ($K_d$ = 70 nM), and

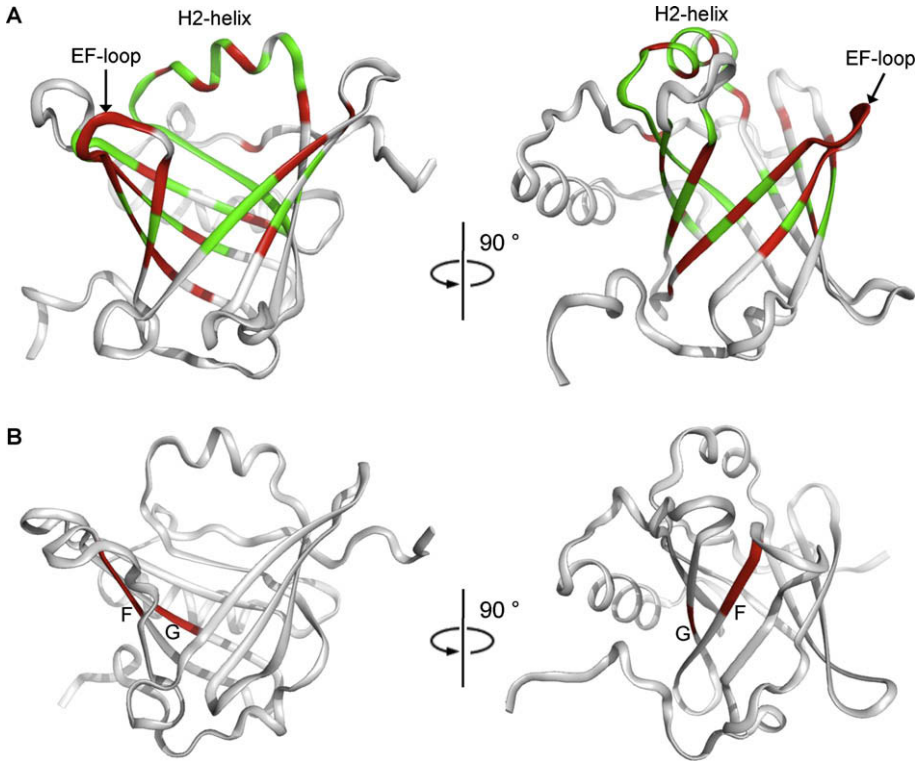


**Fig. 7.** Interactions of L-PGDS and biliverdin. (A) Mapping of NMR signal perturbation on C65A-substituted L-PGDS backbone structure in the presence of 0.3 mM biliverdin. Red and green show the backbone residues with relatively large changes in chemical shift ($\Delta\delta_{tot}$ > 0.10 ppm) and those with signal disappeared upon binding of biliverdin, respectively. In the panels, left and right images are the front and side views of the solution structures of L-PGDS, respectively. (B) Mapping of NMR signal perturbation on C89A/C186A-substituted L-PGDS backbone structure by the binding of all-*trans* retinoic acid (Shimamoto et al., 2007). The protein and the ligand were combined at a molar ratio of 1:1. Backbone residues with relatively large changes in chemical shift ($\Delta\delta_{tot}$ > 0.08 ppm) are colored in red.

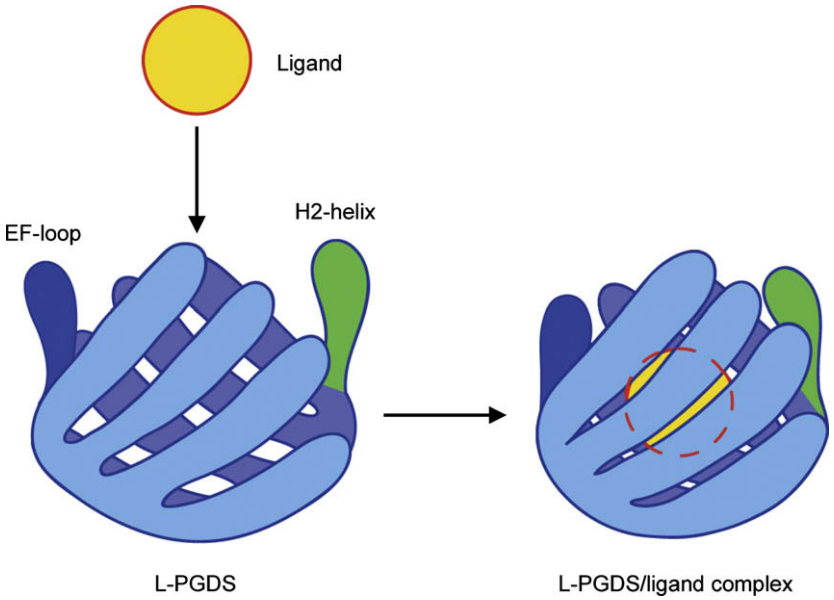


**Fig. 8.** Conceptual illustration of conformational changes of the L-PGDS molecule upon binding of a lipophilic ligand. A small lipophilic ligand enters the large cavity of the β-barrel *via* hydrophobic interactions, then the loops which are located on the edge of the β-barrel lean and the L-PGDS molecule becomes compact. This structural change leads to confinement of the ligand inside the L-PGDS molecule.

18.8 Å for L-PGDS/all-*trans* retinoic acid complex ($K_d$ = 138 nM), indicating that L-PGDS became more compact upon binding biliverdin ($\Delta R_g$ = 1.6 Å) than upon binding all-*trans* retinoic acid ($\Delta R_g$ = 0.6 Å). In addition to the multiple binding modes, the residues that contact with the ligand might become more mobile upon binding biliverdin, resulting in the signal broadening. Actually, the cross-peaks of the residues located in the contact regions were disappeared by the signal broadening, whereas the internal motions of other regions did not change by the binding of biliverdin (Supplementary Fig. 5). In case of bovine β-lactoglobulin, the residues

located at the entrance of the cavity were also disappeared on the 3D NMR spectra upon binding palmitic acid, indicating that the conformational dynamics increased to accommodate each conformation of the bound palmitic acid (Konuma et al., 2007). The conformational entropy could be increased by multiple binding modes and increased mobility so as to achieve the high binding affinity of biliverdin.

L-PGDS is well known to secret into CSF from the leptomeninges and arachnoid membrane (Urade et al., 1993), and is the second most abundant protein constituent in human CSF (Hoffmann et al., 1993; Kuruvilla et al., 1991). Our previous studies showed that the concentration of L-PGDS in CSF increased transiently in patients with SAH in the acute stage and suggested that the purified L-PGDS from the CSF of SAH patients bound bile pigments such as biliverdin and/or its analogs, the metabolites of hemoglobin (Inui et al., 2002; Mase et al., 1999). In addition, the oxidative degradation products of bilirubin and/or biliverdin are one of the causes inducing the delayed vasospasm in patients with SAH (Clark et al., 2002; Kranc et al., 2000; Duff et al., 1988). These lines of evidence suggest that L-PGDS is expected to be a scavenger of the bile pigments that accumulate in the CSF with SAH.

## Acknowledgments

We thank Ms. A. Yamasaki and Mr. T. Bessho for their technical assistance. This study was supported in part by Grants 17300165 and 21500428 (to T.I.) from the program Grants-in-Aid for Scientific Research of the Ministry of Education, Culture, Sports, Science and Technology of Japan and Osaka Prefecture. The synchrotron radiation experiments were performed at the BL40B2 in the SPring-8 with the approval of the Japan Synchrotron Radiation Research Institute (JASRI) (Proposal No. 2006A1059, 2007A1972, 2007A1887, and 2007B1812).

## Appendix A. Supplementary data

Supplementary data associated with this article can be found, in the online version, at doi:10.1016/j.jsb.2009.10.005.

## References

Alving, K., Matran, R., Lundberg, J.M., 1991. The possible role of prostaglandin $D_2$ in the long-lasting airways vasodilatation induced by allergen in the sensitized pig. Acta Physiol. Scand. 143, 93–103.

Bax, A., Delaglio, F., Grzesiek, S., Vuister, G.W., 1994. Resonance assignment of methionine methyl groups and chi 3 angular information from long-range proton–carbon and carbon–carbon J correlation in a calmodulin–peptide complex. J. Biomol. NMR 4, 787–797.

Bertini, I., Cavallaro, G., Luchinat, C., Poli, I., 2003. A use of Ramachandran potentials in protein solution structure determinations. J. Biomol. NMR 26, 355–366.

Beuckmann, C.T., Aoyagi, M., Okazaki, I., Hiroike, T., Toh, H., Hayaishi, O., Urade, Y., 1999. Binding of biliverdin, bilirubin, and thyroid hormones to lipocalin-type prostaglandin D synthase. Biochemistry 38, 8006–8013.

Breustedt, D.A., Korndorfer, I.P., Redl, B., Skerra, A., 2005. The 1.8-Å crystal structure of human tear lipocalin reveals an extended branched cavity with capacity for multiple ligands. J. Biol. Chem. 280, 484–493.

Brunger, A.T., 2007. Version 1.2 of the Crystallography and NMR system. Nat. Protoc. 2, 2728–2733.

Clark, J.F., Reilly, M., Sharp, F.R., 2002. Oxidation of bilirubin produces compounds that cause prolonged vasospasm of rat cerebral vessels: a contributor to subarachnoid hemorrhage-induced vasospasm. J. Cereb. Blood Flow Metab. 22, 472–478.

Cogan, U., Kopelman, M., Mokady, S., Shinitzky, M., 1976. Binding affinities of retinol and related compounds to retinol binding proteins. Eur. J. Biochem. 65, 71–78.

Cornilescu, G., Delaglio, F., Bax, A., 1999. Protein backbone angle restraints from searching a database for chemical shift and sequence homology. J. Biomol. NMR 13, 289–302.

Cowan, S.W., Newcomer, M.E., Jones, T.A., 1990. Crystallographic refinement of human serum retinol binding protein at 2 Å resolution. Proteins Struct. Funct. Genet. 8, 44–61.

Delaglio, F., Grzesiek, S., Vuister, G.W., Zhu, G., Pfeifer, J., Bax, A., 1995. NMRPipe: a multidimensional spectral processing system based on UNIX pipes. J. Biomol. NMR 6, 277–293.

Dempsey, C.E., 2001. Hydrogen exchange in peptides and proteins using NMR-spectroscopy. Prog. Nucl. Magn. Reson. Spectrosc. 39, 135–170.

Duff, T.A., Feilbach, J.A., Yusuf, Q., Scott, G., 1988. Bilirubin and the induction of intracranial arterial spasm. J. Neurosurg. 69, 593–598.

Dumitrascu, D., 1996. Mast cells as potent inflammatory cells. Rom. J. Intern. Med. 34, 159–172.

Eichinger, A., Nasreen, A., Kim, H.J., Skerra, A., 2007. Structural insight into the dual ligand specificity and mode of high density lipoprotein association of apolipoprotein D. J. Biol. Chem. 282, 31068–31075.

Flower, D.R., 1996. The lipocalin protein family: structure and function. Biochem. J. 318, 1–14.

Flower, D.R., North, A.C., Sansom, C.E., 2000. The lipocalin protein family: structural and sequence overview. Biochim. Biophys. Acta 1482, 9–24.

Fukuhara, N., Fernandez, E., Ebert, J., Conti, E., Svergun, D., 2004. Conformational variability of nucleo-cytoplasmic transport factors. J. Biol. Chem. 279, 2176–2181.

Ganforina, M.D., Gutiérrez, G., Bastiani, M., Sanchez, D., 2000. A phylogenetic analysis of the lipocalin protein family. Mol. Biol. Evol. 17, 114–126.

Grunewald, S., Huyben, K., de Jong, J.G., Smeitink, J.A., Rubio, E., Boers, G.H., Conradt, H.S., Wendel, U., Wevers, R.A., 1999. Beta-trace protein in human cerebrospinal fluid: a diagnostic marker for *N*-glycosylation defects in brain. Biochim. Biophys. Acta 1455, 54–60.

Guinier, A., Fournet, G., 1955. Small-Angle Scattering of X-rays. Wiley, New York.

Hajjar, E., Perahia, D., Debat, H., Nespoulous, C., Robert, C.H., 2006. Odorant binding and conformational dynamics in the odorant-binding protein. J. Biol. Chem. 281, 29929–29937.

Harrington, M.G., Aebersold, R., Martin, B.M., Merril, C.R., Hood, L., 1993. Identification of a brain-specific human cerebrospinal fluid glycoprotein, beta-trace protein. Appl. Theor. Electrophor. 3, 229–234.

Hoffmann, A., Conradt, H.S., Gross, G., Nimtz, M., Lottspeich, F., Wurster, U., 1993. Purification and chemical characterization of beta-trace protein from human cerebrospinal fluid: its identification as prostaglandin D synthase. J. Neurochem. 61, 451–456.

Iida, T., Nishimura, S., Mochizuki, M., Uchiyama, S., Ohkubo, T., Urade, Y., Tanaka, A., Inui, T., 2008. Thermal unfolding mechanism of lipocalin-type prostaglandin D synthase. FEBS J. 275, 233–241.

Inoue, K., Oka, T., Miura, K., Yagi, N., 2004. Present status of BL40B2 and BL40XU at SPring-8 (Beamlines for small angle X-ray scattering). AIP Conf. Proc. 705, 336–339.

Inoue, K., Yagi, N., Urade, Y., Inui, T., 2009. Compact packing of lipocalin-type prostaglandin D synthase induced by binding of lipophilic ligands. J. Biochem. 145, 169–175.

Inui, T., Mase, M., Emi, M., Nakau, H., Seiki, K., Oda, H., Yamada, K., Urade, Y., 2002. Lipocalin-type prostaglandin D synthase in cerebrospinal fluid of patients with aneurysmal subarachnoid hemorrhage scavenges bile pigments. Int. Congr. Ser. 1233, 447–451.

Inui, T., Ohkubo, T., Emi, M., Irikura, D., Hayaishi, O., Urade, Y., 2003. Characterization of the unfolding process of lipocalin-type prostaglandin D synthase. J. Biol. Chem. 278, 2845–2852.

Inui, T., Ohkubo, T., Urade, Y., Hayaishi, O., 1999. Enhancement of lipocalin-type prostaglandin D synthase enzyme activity by guanidine hydrochloride. Biochem. Biophys. Res. Commun. 266, 641–646.

Kanekiyo, T., Ban, T., Aritake, K., Huang, Z.L., Qu, W.M., Okazaki, I., Mohri, I., Murayama, S., Ozono, K., Taniike, M., Goto, Y., Urade, Y., 2007. Lipocalin-type prostaglandin D synthase/beta-trace is a major amyloid beta-chaperone in human cerebrospinal fluid. Proc. Natl. Acad. Sci. USA 104, 6412–6417.

Kay, L.E., 1995. Pulsed field gradient multi-dimensional NMR methods for the study of protein structure and dynamics in solution. Prog. Biophys. Mol. Biol. 63, 277–299.

Konuma, T., Sakurai, K., Goto, Y., 2007. Promiscuous binding of ligands by beta-lactoglobulin involves hydrophobic interactions and plasticity. J. Mol. Biol. 368, 209–218.

Koradi, R., Billeter, M., Wuthrich, K., 1996. MOLMOL: a program for display and analysis of macromolecular structures. J. Mol. Graph. 14 (51–55), 29–32.

Kozin, M.I., Svergun, D.I., 2001. Automated matching of high- and low-resolution structural models. J. Appl. Crystallogr. 34, 33–41.

Kranc, K.R., Pyne, G.J., Tao, L., Claridge, T.D., Harris, D.A., Cadoux-Hudson, T.A., Turnbull, J.J., Schofield, C.J., Clark, J.F., 2000. Oxidative degradation of bilirubin produces vasoactive compounds. Eur. J. Biochem. 267, 7094–7101.

Kuruvilla, A.P., Hochwald, G.M., Ghiso, J., Castano, E.M., Pizzolato, M., Frangione, B., 1991. Isolation and amino terminal sequence of beta-trace, a novel protein from human cerebrospinal fluid. Brain Res. 565, 337–340.

Laskowski, R.A., Rullmannn, J.A., MacArthur, M.W., Kaptein, R., Thornton, J.M., 1996. AQUA and PROCHECK-NMR: programs for checking the quality of protein structures solved by NMR. J. Biomol. NMR 8, 477–486.

Mase, M., Yamada, K., Iwata, A., Matsumoto, T., Seiki, K., Oda, H., Urade, Y., 1999. Acute and transient increase of lipocalin-type prostaglandin D synthase (beta-trace) level in cerebrospinal fluid of patients with aneurysmal subarachnoid hemorrhage. Neurosci. Lett. 270, 188–190.

Mase, M., Yamada, K., Shimazu, N., Seiki, K., Oda, H., Nakau, H., Inui, T., Li, W., Eguchi, N., Urade, Y., 2003. Lipocalin-type prostaglandin D synthase (beta-trace) in cerebrospinal fluid: a useful marker for the diagnosis of normal pressure hydrocephalus. Neurosci. Res. 47, 455–459.

Matsuoka, T., Hirata, M., Tanaka, H., Takahashi, Y., Murata, T., Kabashima, K., Sugimoto, Y., Kobayashi, T., Ushikubi, F., Aze, Y., Eguchi, N., Urade, Y., Yoshida,

N., Kimura, K., Mizoguchi, A., Honda, Y., Nagai, H., Narumiya, S., 1995. Prostaglandin $D_2$ as a mediator of allergic asthma. Science 287, 2013–2017.
McPhee, F., Caldera, P.S., Bemis, G.W., McDonagh, A.F., Kuntz, I.D., Craik, C.S., 1996. Bile pigments as HIV-1 protease inhibitors and their effects on HIV-1 viral maturation and infectivity in vitro. Biochem. J. 320, 681–686.
Mohri, I., Taniike, M., Okazaki, I., Kagitani-Shimono, K., Aritake, K., Kanekiyo, T., Yagi, T., Takikita, S., Kim, H.S., Urade, Y., Suzuki, K., 2006. Lipocalin-type prostaglandin D synthase is up-regulated in oligodendrocytes in lysosomal storage diseases and binds gangliosides. J. Neurochem. 97, 641–651.
Pattanayek, R., Newcomer, M.E., 1999. Protein and ligand adaptation in a retinoic acid binding protein. Protein Sci. 8, 2027–2032.
Pervaiz, S., Brew, K., 1987. Homology and structure-function correlations between $\alpha_1$-acid glycoprotein and serum retinol-binding protein and its relatives. FASEB J. 1, 209–214.
Piotto, M., Saudek, V., Sklenar, V., 1992. Gradient-tailored excitation for single-quantum NMR spectroscopy of aqueous solutions. J. Biomol. NMR 2, 661–665.
Saso, L., Leone, M.G., Sorrentino, C., Giacomelli, S., Silvestrini, B., Grima, J., Li, J.C., Samy, E., Mruk, D., Cheng, C.Y., 1998. Quantification of prostaglandin D synthetase in cerebrospinal fluid: a potential marker for brain tumor. Biochem. Mol. Biol. Int. 46, 643–656.
Shimamoto, S., Yoshida, T., Inui, T., Gohda, K., Kobayashi, Y., Fujimori, K., Tsurumura, T., Aritake, K., Urade, Y., Ohkubo, T., 2007. NMR solution structure of lipocalin-type prostaglandin D synthase: evidence for partial overlapping of catalytic pocket and retinoic acid-binding pocket within the central cavity. J. Biol. Chem. 282, 31373–31379.
Svergun, D.I., 1992. Determination of the regularization parameter in indirect-transform methods using perceptual criteria. J. Appl. Crystallogr. 25, 495–503.
Svergun, D.I., Barberato, C., Koch, M.H.J., 1995. CRYSOL – a program to evaluate X-ray solution scattering of biological macromolecules from atomic coordinates. J. Appl. Crystallogr. 28, 768–773.
Svergun, D.I., 1999. Restoring low resolution structure of biological macromolecules from solution scattering using simulated annealing. Biophys. J. 76, 2879–2886.
Svergun, D.I., Petoukhov, M.V., Koch, M.H., 2001. Determination of domain structure of proteins from X-ray solution scattering. Biophys. J. 80, 2946–2953.
Tanaka, T., Urade, Y., Kimura, H., Eguchi, N., Nishikawa, A., Hayaishi, O., 1997. Lipocalin-type prostaglandin D synthase (beta-trace) is a newly recognized type of retinoid transporter. J. Biol. Chem. 272, 15789–15795.
Tumani, H., Nau, R., Felgenhauer, K., 1998. Beta-trace protein in cerebrospinal fluid: a blood–CSF barrier-related evaluation in neurological diseases. Ann. Neurol. 44, 882–889.
Urade, Y., Eguchi, N., 2002. Lipocalin-type and hematopoietic prostaglandin D synthases as a novel example of functional convergence. Prostaglandins Other Lipid Mediators 68–69, 375–382.
Urade, Y., Hayaishi, O., 2000a. Biochemical, structural, genetic, physiological, and pathophysiological features of lipocalin-type prostaglandin D synthase. Biochim. Biophys. Acta 1482, 259–271.
Urade, Y., Hayaishi, O., 2000b. Prostaglandin D synthase: structure and function. Vitam. Horm. 58, 89–120.
Urade, Y., Kitahama, K., Ohishi, H., Kaneko, T., Mizuno, N., Hayaishi, O., 1993. Dominant expression of mRNA for prostaglandin D synthase in leptomeninges, choroid plexus, and oligodendrocytes of the adult rat brain. Proc. Natl. Acad. Sci. USA 90, 9070–9074.
Volkov, V.V., Svergun, D.I., 2003. Uniqueness of *ab initio* shape determination in small-angle scattering. J. Appl. Crystallogr. 36, 860–864.
Wüthrich, K., 1986. NMR of Proteins and Nucleic Acids. John Wiley, New York.
Wishart, D.S., Bigam, C.G., Holm, A., Hodges, R.S., Sykes, B.D., 1995. $^{1}H$, $^{13}C$ and $^{15}N$ random coil NMR chemical shifts of the common amino acids. I. Investigations of nearest-neighbor effects. J. Biomol. NMR 5, 67–81.
Yamazaki, T., Formankay, J.D., Kay, L.E., 1993. Two-dimensional NMR experiments for correlating $^{13}C\beta$ and $^{1}H$-$\delta/\varepsilon$ chemical-shifts of aromatic residues in $^{13}C$-labeled proteins via scalar couplings. J. Am. Chem. Soc. 115, 11054–11055.